

Some basics on Graphene

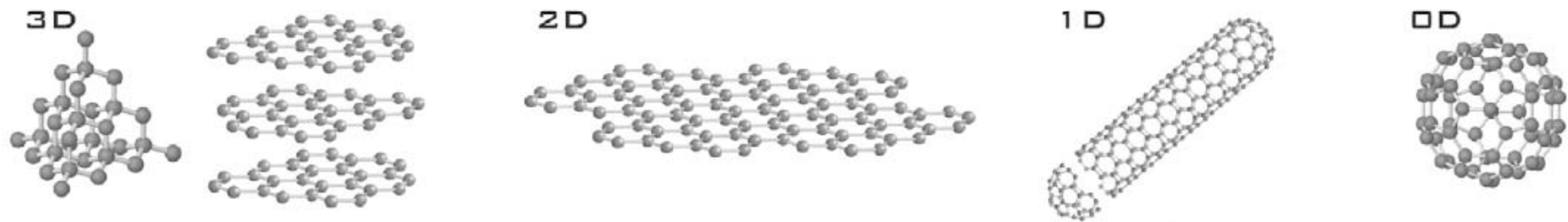


Fig. 1 Crystal structures of the different allotropes of carbon. (Left to right) Three-dimensional diamond and graphite (3D); two-dimensional graphene (2D); one-dimensional nanotubes (1D); and zero-dimensional buckyballs (0D). (Adapted and reprinted with permission from⁶⁶. © 2002 Prentice Hall.)

Graphene is the name given to a single layer of carbon atoms densely packed into a benzene-ring structure [1].

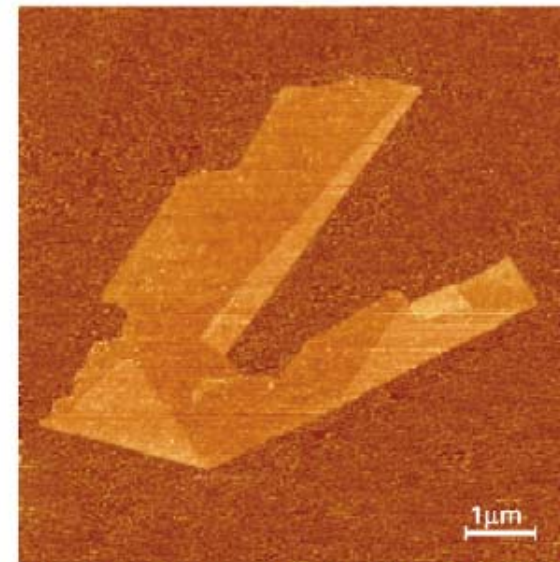
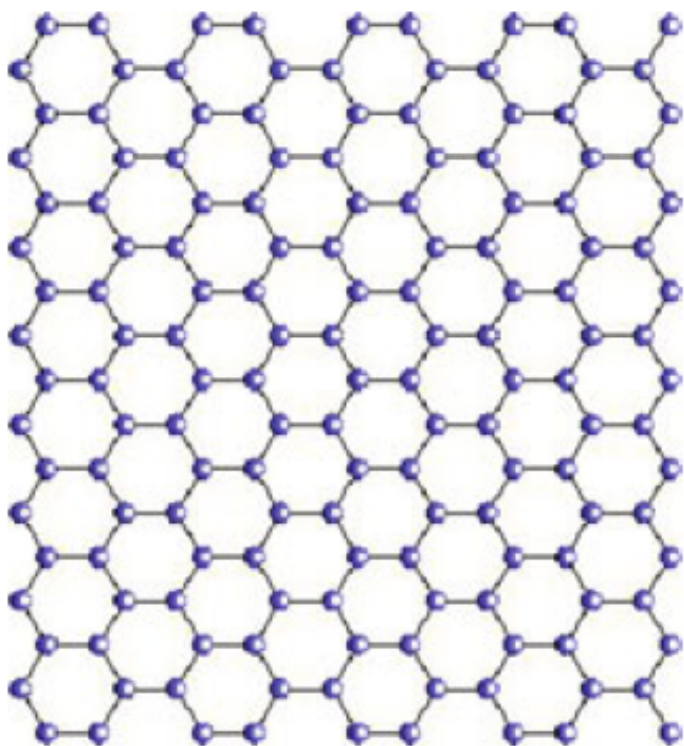
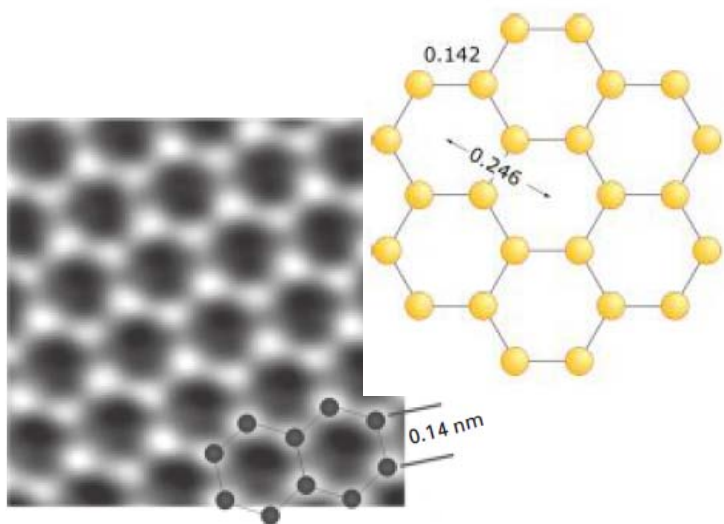
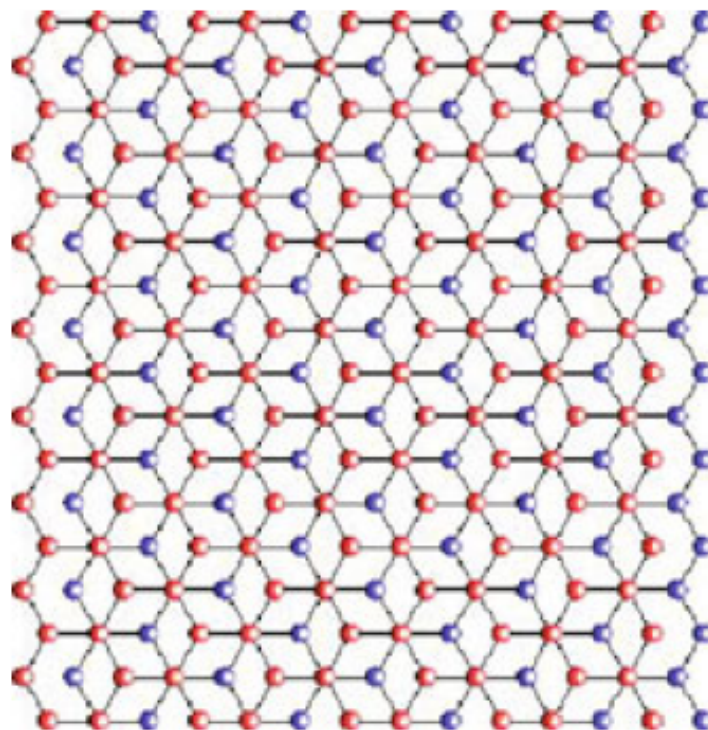


Fig. 2 Atomic force microscopy image of a graphene crystal on top of an oxidized Si substrate. Folding of the flake can be seen. The measured thickness of graphene corresponds to the interlayer distance in graphite. Scale bar = 1 μm. (Reprinted with permission from¹³. © 2005 National Academy of Sciences.)

Graphene



Bilayer Graphene



In realtà il Grafene rappresenta molto più di un cristallo bidimensionale, poiché in soli 0.34 nm di spessore sono racchiuse così tante proprietà non comuni a nessun altro materiale che sin da subito hanno catturato l'attenzione dell'intera comunità scientifica. Nell'ottobre 2010, a distanza di pochi anni dai primi *esperimenti innovativi riguardanti il grafene*, l'idea di **Andre Geim** e **Kostantin Novoselov** è stata premiata con il Nobel per la Fisica [2, 3].

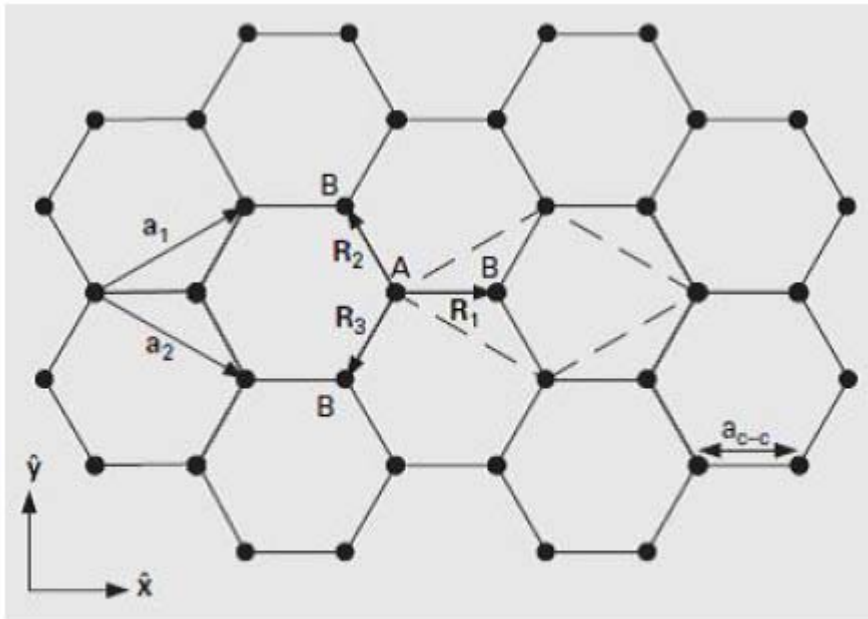


Figura 1.9: reticolo del Grafene [8].

$$\vec{a}_1 = \left(\frac{\sqrt{3}a}{2}, \frac{a}{2} \right)$$

$$\vec{a}_2 = \left(\frac{\sqrt{3}a}{2}, \frac{-a}{2} \right)$$

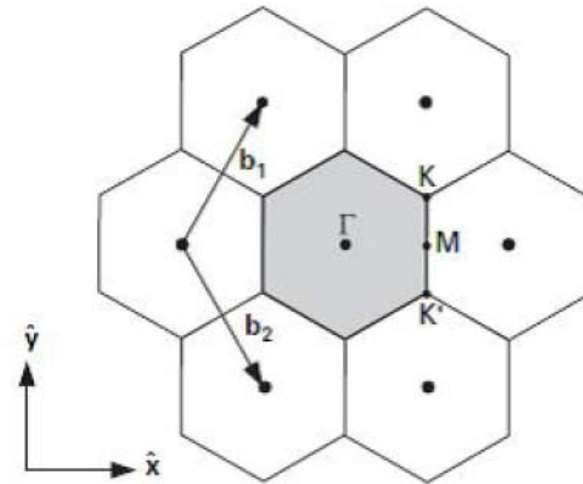


Figura 1.10: Reticolo reciproco del reticolo cristallino a nido d'ape [8].

Con $|\Gamma M| = \frac{2\pi}{\sqrt{3}a}$, $|\Gamma K| = \frac{4\pi}{3a}$ e $|MK| = \frac{2\pi}{3a}$. All'interno

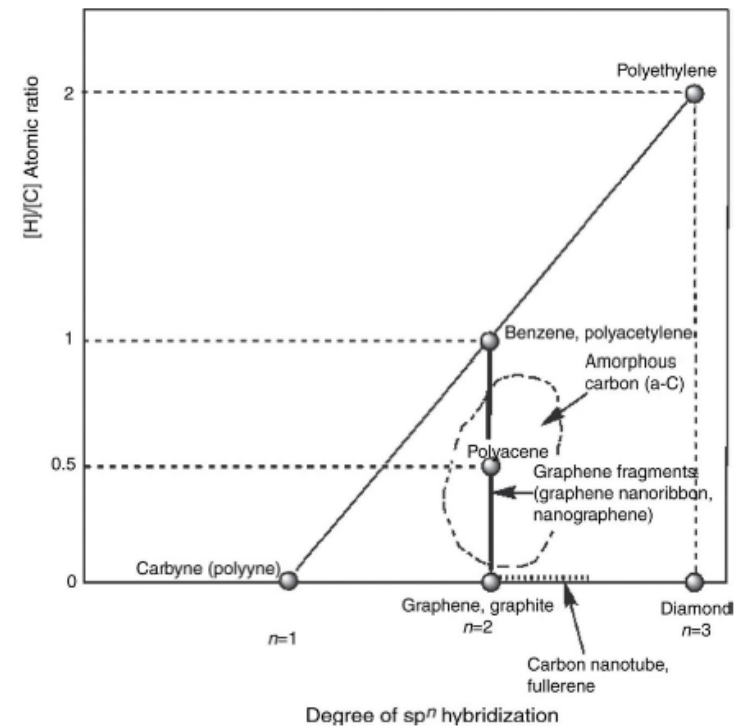
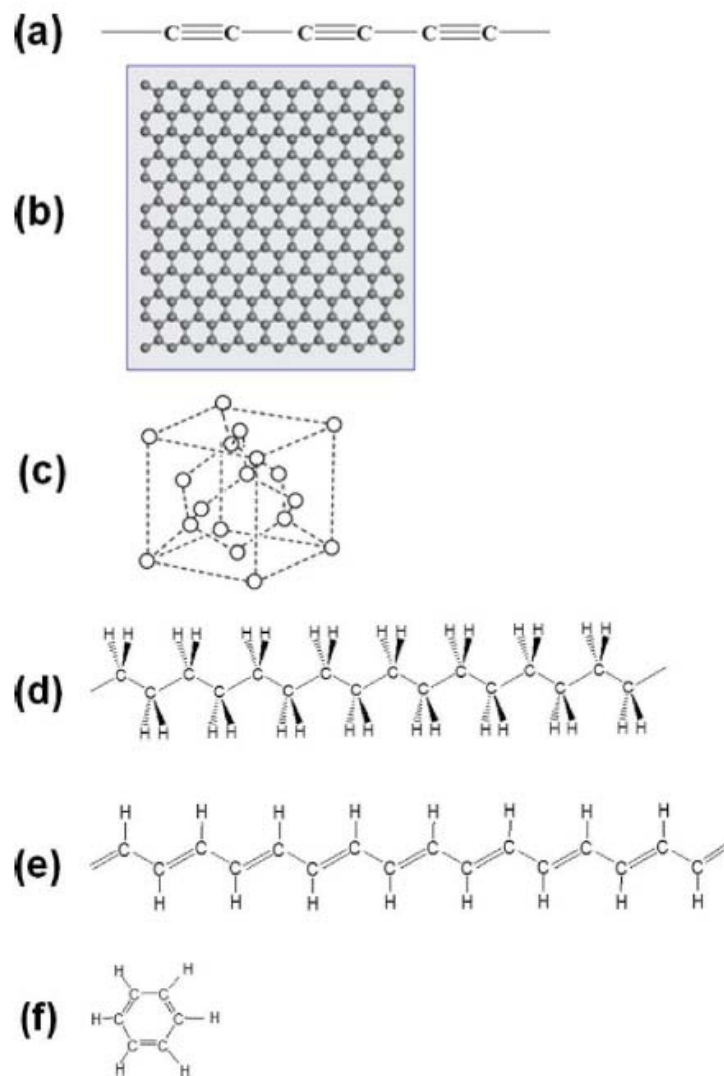
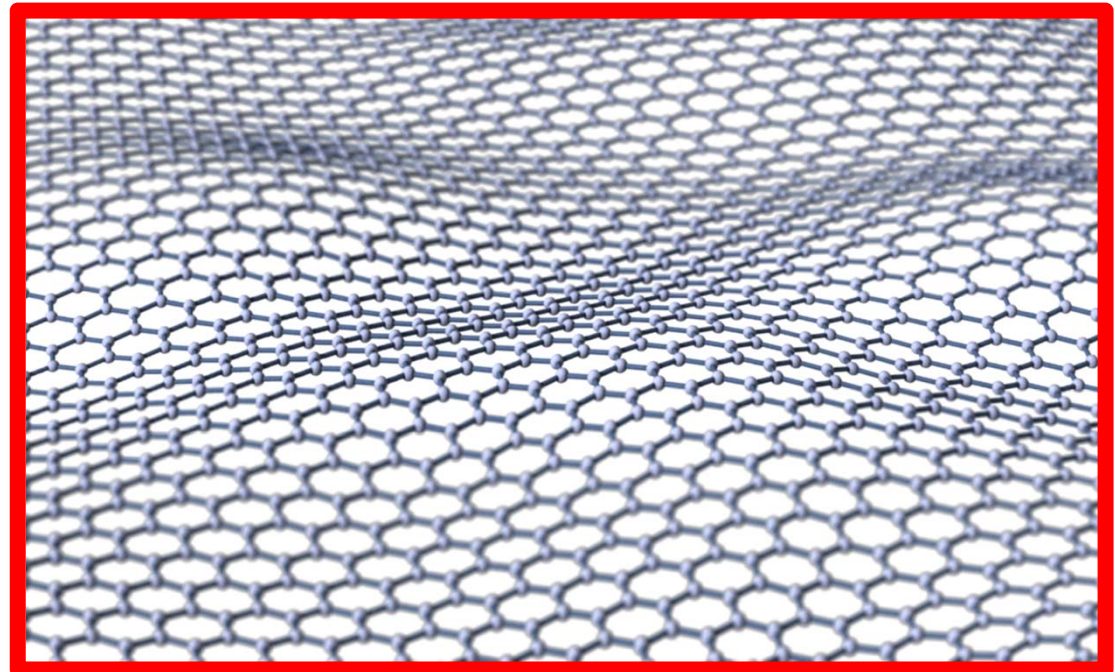
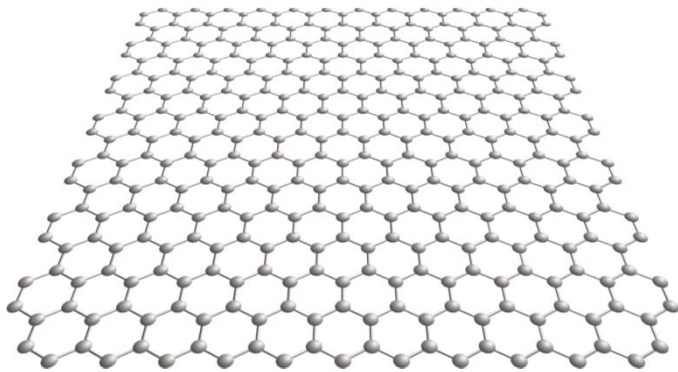


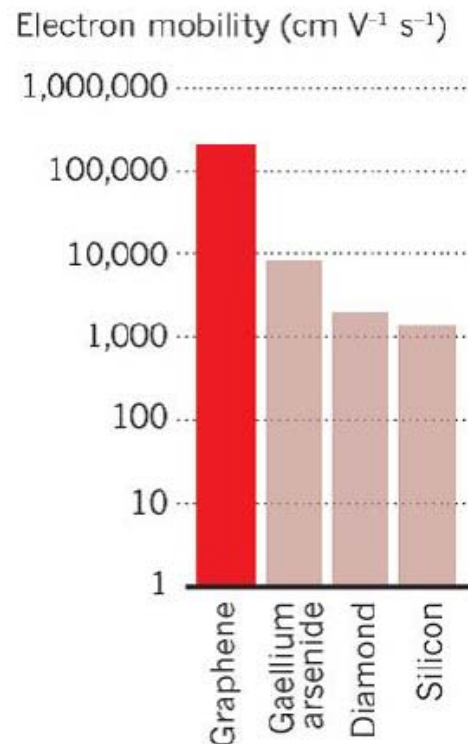
Figura 1.2: strutture atomiche dei vari materiali di Carbonio: (a) Polirene, (b) Grafene, (c) Diamante, (d) Politelene, (e) Poliacetilene, (f) Benzene [1].

I primi lavori sulla struttura a bande del singolo piano di grafite sono datati al periodo tra il 1947 ed il 1958, anche se il grafene continuava ad essere considerato un puro esercizio accademico, poiché gli stessi studi mostravano l'impossibilità di ottenere sistemi strettamente bidimensionali, stabili allo stato isolato [5, 6, 7].



Osservando la sua dispersione energetica si osserva che gli elettroni e le lacune si comportano come particelle a massa nulla [8].

In un semiconduttore la mobilità dei portatori di carica é inversamente proporzionale alla massa efficace; nel caso del Grafene, essendo gli elettroni liberi di muoversi come particelle prive di massa, avranno una mobilità estremamente elevata rendendo il Grafene un ottimo conduttore elettrico. Dai dati sperimentali si osserva che il comportamento



In a nutshell, the results suggested that graphene is a semi-metal, i.e. it has zero bandgap, with linear dispersion around the chemical potential leading to cones in two-dimensional reciprocal space. This was quite a surprising result because most of the matter waves have quadratic dispersions following Schrödinger equation, which is first order in time and second order in space. In the simplest model, it leads to the following dispersion for the conduction and valence bands, respectively:

$$E_S(\mathbf{k}) = E_{c,v} + \frac{\hbar^2 |\mathbf{k}|^2}{2m_{c,v}} \quad (1.1)$$

where $E_{c,v}$ are the conduction and valence band edges and $m_{c,v}$ are the effective masses of electrons in conduction band and holes in valence band, respectively (m_v is negative, $S \equiv \textit{Schrödinger}$). One gets zero bandgap for $E_c = E_v$; however, the dispersion still remains quadratic.

In contrast to the Schrödinger equation, the dispersion for the Dirac equation is

$$E_D(\mathbf{k}) = \pm \sqrt{m^2c^4 + \hbar^2c^2|\mathbf{k}|^2}, \quad (1.2)$$

where c is the speed of light and m is the relativistic mass ($D \equiv Dirac$). The positive and negative dispersion plots are shown in Fig. 1.2, which give rise to a mass-dependent gap of $2mc^2$ between the positive energy of matter (electron in this case) and the negative energy of anti-matter (positron) – the mc^2 product for an electron is about 0.512 MeV. In the limiting case of $m = 0$, clearly the gap becomes zero. Furthermore, (1.2) becomes

$$E_D(\mathbf{k}) = \pm \hbar c |\mathbf{k}| \quad (1.3)$$

which is plotted in Fig. 1.2 depicting the linear dispersion with zero bandgap, the energy scale on the order of MeV and the speed equal to that of light.

Tale eq.1.12 é plottata nella Fig.1.11, in cui i punti speciali K e K' sono anche detti *punti di Dirac* e vicino ai quali la dispersione energetica é lineare secondo l'equazione:

$$E(\mathbf{k}) = \mp \hbar v_F |\mathbf{k}| \quad (1.13)$$

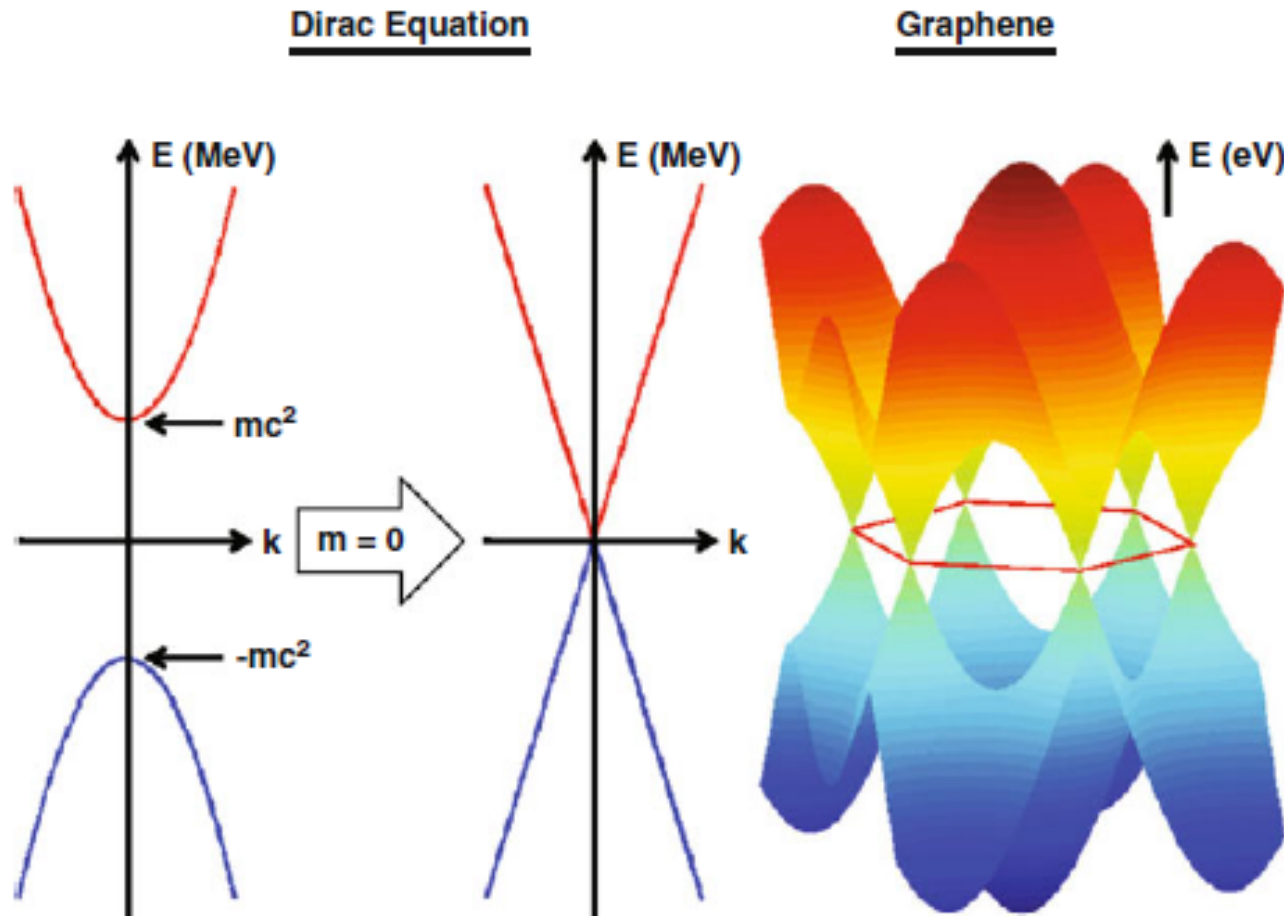


Fig. 1.2 Graphene band structure. Dirac dispersions with $2mc^2$ gap are shown. In the limit of $m = 0$, the gap becomes zero with a linear dispersion, where the energy scale is on the order of MeV. In analogy, the graphene band structure also has a linear dispersion with zero gap around the Dirac point, albeit with the energy in eV range

As a reference, the band structure of graphene is shown in Fig. 1.2, which follows the following equation based on tight-binding description [2]:

$$E_G(k) = \pm t \sqrt{1 + 4 \cos\left(\frac{3k_x a_{cc}}{2}\right) \cos\left(\frac{\sqrt{3}k_y a_{cc}}{2}\right) + 4 \cos^2\left(\frac{\sqrt{3}k_y a_{cc}}{2}\right)},$$

t=2.75 eV

(1.4)

where $a_{cc} = 1.42 \text{ \AA}$ is the C–C bond length and t is the first nearest-neighbour tight-binding parameter ($G \equiv \textit{graphene}$). Clearly the bandgap is zero and dispersion is linear around the points where conduction and valence bands meet with a renormalized velocity v resulting in

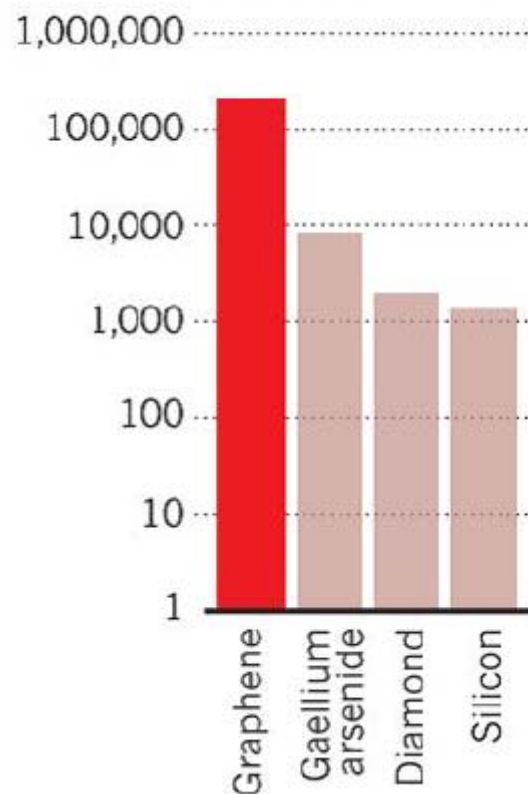
$$E_G(k) = \pm \hbar v |k|$$
(1.5)

similar to the dispersion of Dirac's in (1.3). Readers are encouraged to see Chap. 8

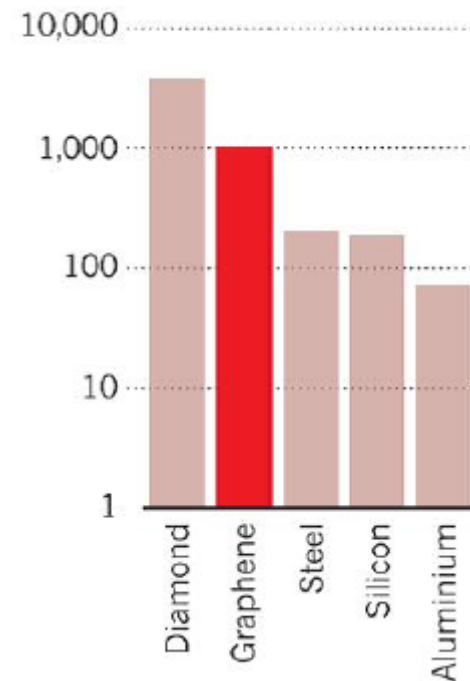
- $v_F = \frac{3ta}{2\hbar} \cong \frac{c}{300}$ (velocità di Fermi).
- $k = (k_x, k_y)$ il vettore d'onda;

La dispersione energetica (cosí ottenuta) implica che gli elettroni e le lacune si comportino come particelle a massa nulla e le loro disposizioni siano perfettamente simmetriche intorno al *punto di Dirac* (Fig 1.13).

Electron mobility ($\text{cm V}^{-1} \text{s}^{-1}$)



Stiffness (Young's modulus, GPa)



Question 1: defects

co. Dai dati sperimentali si osserva che il comportamento del Grafene si discosta notevolmente dalle predizioni teoriche, poiché il materiale analizzato in laboratorio presenta difetti reticolari (in un numero a volte significativo) e tipicamente i processi necessari alla sua sintesi lasciano diverse contaminazioni chimiche sulla superficie, rendendo il materiale significativamente diverso dal punto di vista delle proprietà chimiche o fisiche.

Question 2: metal contacting

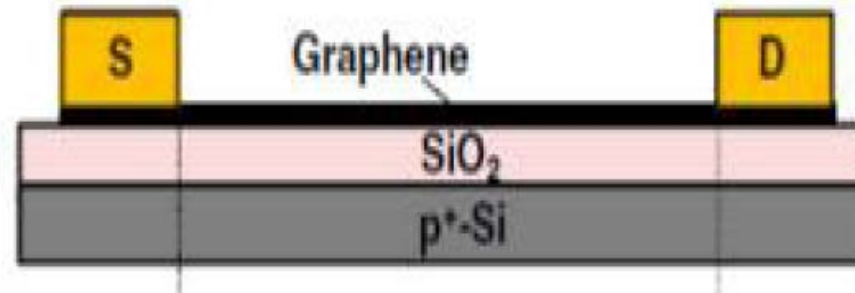
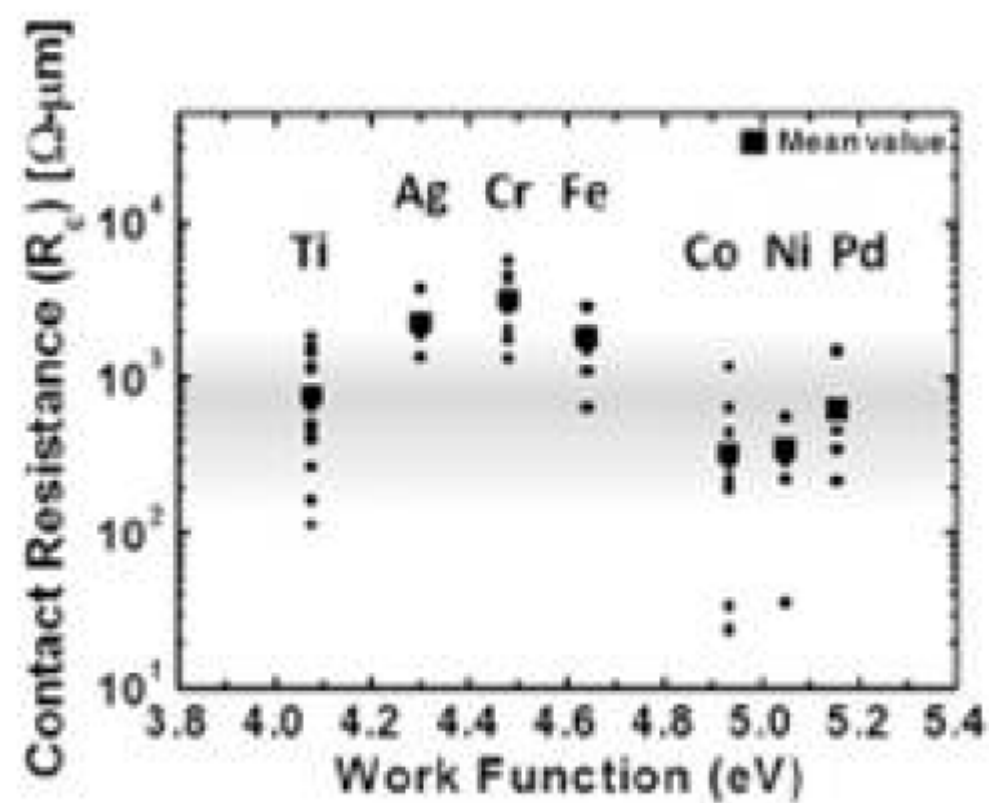


Figura 1: Una struttura tipica del Grafene cresciuto su un'ossido e contattato con due metalli [9].

Se viene fornita una **d.d.p.** tra il *Source* e il *Drain* nella struttura presente nella Fig.1, si osserva un passaggio di corrente e così si procede nel calcolo della resistenza totale R_{total} che è funzione della *d.d.p.* fornita al sistema (Fig.3).

La R_{total} è possibile scriverla come: $R_{total} = 2R_C + R_g$ [9].

- R_C è la resistenza di contatto fra il metallo e il Grafene.
- R_g è la resistenza del grafene dove funge da canale di elettroni.



Interaction of Au atoms with graphene; Mobility of Au atoms on graphene

A.1) Theoretical data state that the Au–Au interaction is significantly stronger than the Au–graphene interaction and for this reason Au is highly mobile on graphene.

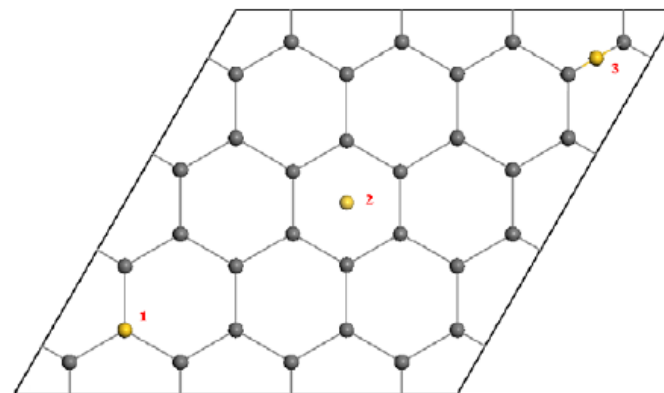


Figure 1. The initial positions of gold atoms on graphene: (1) atop, directly above a carbon atom; (2) hollow, directly above the centre of a hexagon of carbon atoms; (3) bridge, directly above a carbon–carbon bond.

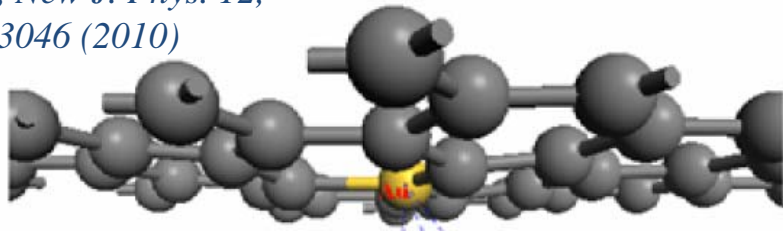
Table 1. Interaction between a gold adatom and a graphene surface. E_B is the binding energy. h is the height of the gold atom above the nearest carbon atom.

Site	$-E_B$ (eV)	h (nm)	Au charge (e)	Au moment (μ_B)
Atop	0.79	0.244	+0.15	-0.15
Bridge	0.74	0.227	+0.17	-0.17
Hollow	0.52	0.226	+0.11	-0.11

$-E_B(\text{Au-Au}) \sim 1$ eV (P. K. Jain, Structural Chemistry 16, 421 (2005))

In-plane diffusion

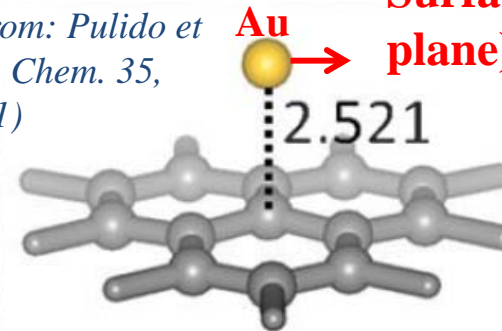
Adapted from: Mao et al., *New J. Phys.* 12, 033046 (2010)



$$E_{A(IN)} = E_{VACANCY\ FORMATION} + E_{MIGRATION}$$

Surface (on-plane) diffusion

Adapted from: Pulido et al., *New J. Chem.* 35, 2153 (2011)



$$E_{A(ON)} = E_{MIGRATION}$$

Some estimations

$$D_{S0} = 8.2 \times 10^{-8} \text{ cm}^2/\text{s}$$

An estimation of the attempt frequency

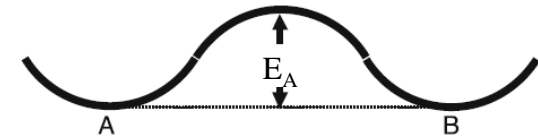
$$D_{S0} = ga^2 \nu_0 \rightarrow \nu_0 = 1.3 \times 10^8 \text{ s}^{-1} \rightarrow t_0 = 7.7 \text{ ns}$$

[$g \sim 1$ a geometrical factor
 $a = 2.46 \text{ \AA}$ the graphene lattice constant
S. Malola et al., Appl. Phys. Lett. 94, 043106 (2009)]

An estimation of the jump frequency at 500 °C

$$\nu(T) = \nu_0 \exp\left(-\frac{E_A}{kT}\right) = 1.3 \times 10^6 \text{ s}^{-1} \rightarrow t = 77 \text{ \mu s}$$

$$[\text{jump probability } P(500 \text{ °C}) = \exp\left(-\frac{E_A}{kT}\right) = 0.01]$$



Furthermore, the size of Au is too large to match the graphene lattice. Metal with a nearest neighbor distance of 0.27 nm can perfectly fit the graphene lattice (0.245 nm) based on experimental results. **The nearest-neighbor distance for Au is 0.288 nm, making it difficult to fit the graphene lattice.**

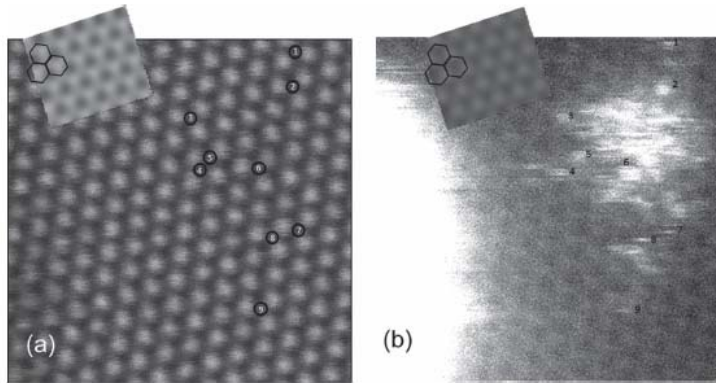


Figure 3. a) BF and b) HAADF STEM images of 0.5 nm gold evaporated on few-layer graphene. In the HAADF image individual gold atoms can be seen to have separated from a gold cluster on the left-hand side. Identical positions of the benzene rings are marked in black in the image simulations overlaid on the experimental images, which show that bright contrast in the BF image and dark contrast in the HAADF image correspond to the centers of benzene rings. Single-atom positions 1–9 are marked with numbers just to the right of the bright atoms in the HAADF image; identical places are marked by circles with the numbers inside in the BF image, which shows that Au atoms sit on T sites on the sample surface. All images represent raw, unfiltered data. The frame width is 3 nm.

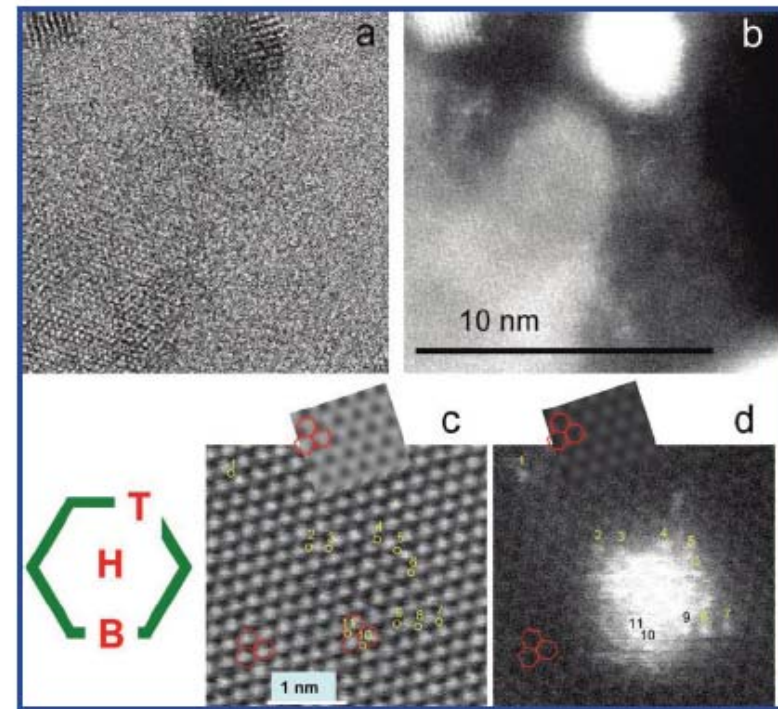


Figure 2. (a) BF STEM image of 0.2 Å gold evaporated on graphene, showing a monolayer gold-atom raft in the left bottom corner and a gold nanocrystal at the top. (b) Corresponding HAADF image. (c) Atomic resolution BF and (d) corresponding HAADF STEM image depicting a few-layer patch in graphene evaporated with 5 Å of gold. In (d) individual gold atoms can be seen separated from the small cluster in the middle. Benzene rings are overlaid in red in both images, showing that bright contrast in the BF image corresponds to dark contrast in the centers of the top-layer benzene rings in the HAADF image, as derived from simulations of three-layer graphene (at -50 Å defocus), shown in the insets in (c) and (d). Single atoms are marked with numbers 1–11 just above the atoms in the HAADF image; identical places are marked by yellow circles in the BF image, identifying them to be T sites. The images represent raw, unfiltered data. Shown on the left of (c) is a schematic with metal sites on the benzene ring.

Growth of metal clusters and thin films on graphene

During the growth, Pt, W, and Re form epitaxial cluster superlattices while Fe and Au do not. Metals which grow epitaxial cluster superlattices have three characteristics: (i) a large cohesive strength to form strong bonds; (ii) a large extension of a localized valence orbital to efficiently interact with graphene and thus to initiate rehybridization of carbon atoms; and (iii) a certain match with the graphene unit cell. **Au atoms, instead, form large 3D clusters on graphene due to the weak interaction between Au and carbon.**

Table 1
Metal-carbon bond dissociation energies [16,17].

Metal	D(M-C), kJ/mol
Ir	631
Pt	610
Rh	580
Pd	436
Co	347

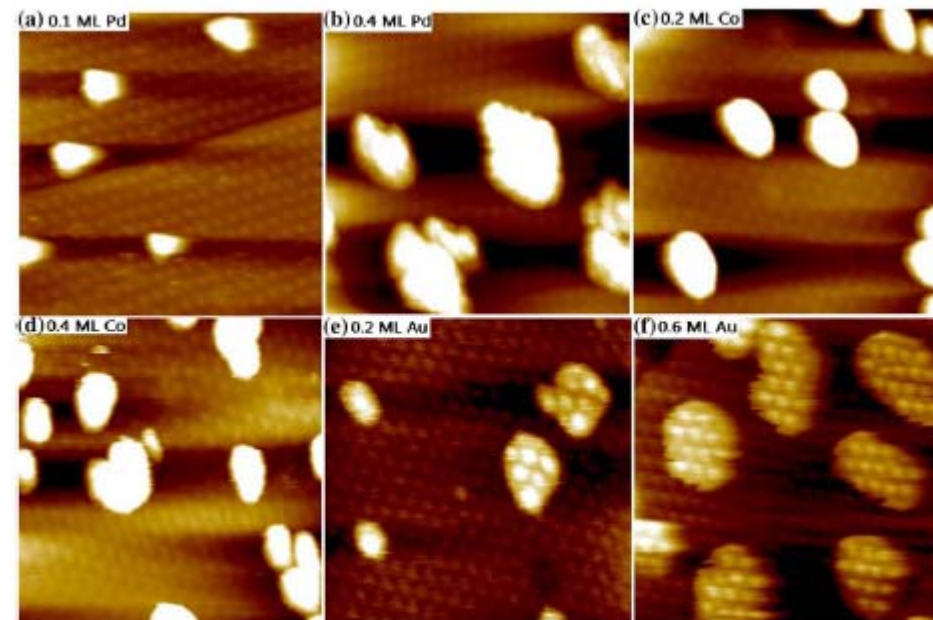
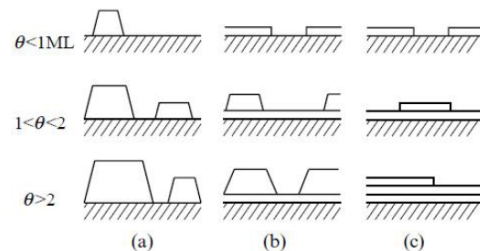


Fig. 6. STM images (50 nm × 50 nm, $V_b = 1.0$ V, $I_t = 0.1$ nA) of (a) 0.1 ML Pd, (b) 0.4 ML Pd, (c) 0.2 ML Co, (d) 0.4 ML Co, (e) 0.2 ML Au and (f) 0.6 ML Au deposited on graphene/Ru(0001) at room temperature.

Figura 1.16: Rappresentazione dei tre modi di crescita in funzione della quantità di materiale depositato (θ). (a) isole, o crescita Volmer-Weber; (b) layer-isole, o crescita Stranski-Krastanov; (c) layer-by-layer, o crescita Frank-van der Merwe [12].

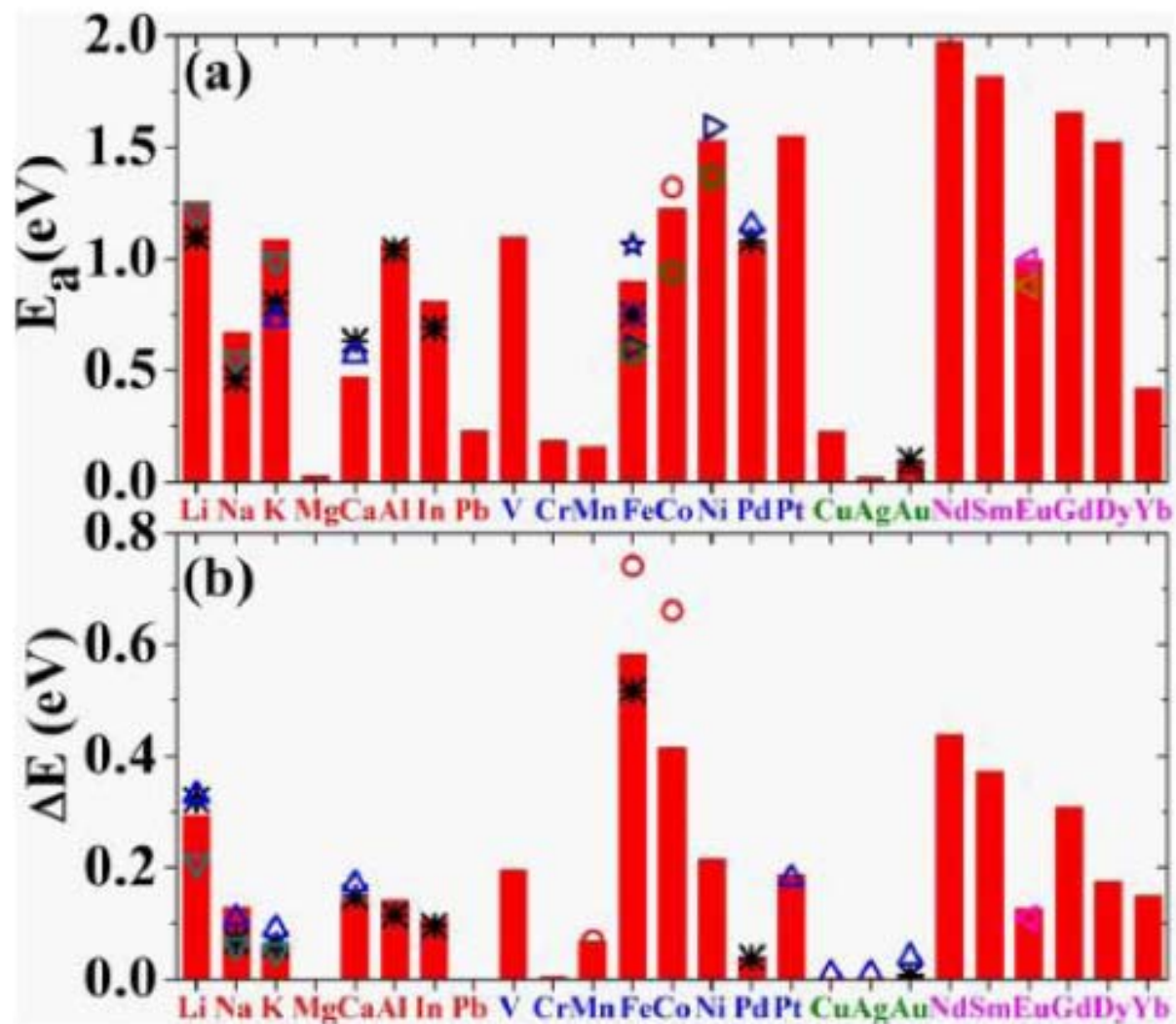


Figura 1.23: (a) L'energia di adsorbimento dei vari metalli cresciuti sul Grafene. (b) la barriera di diffusione [19].

Confrontando la crescita morfologica dei metalli al di sopra del Grafene si é visto che essa dipende fortemente dall'energia di adsorbimento, in particolare dal rapporto $\frac{E_a}{E_c}$ presente in Fig.1.24 (E_c é l'energia di coesione fra il *metallo bulk* e il *Grafene*).

- Se $\frac{E_a}{E_c} \cong 1$ allora i Cluster di metallo crescono in strutture bidimensionali (crescita Frank-van der Merwe).
- Se $\frac{E_a}{E_c} \ll 1$ allora i Cluster di metallo crescono in strutture tridimensionali (Volmer-Weber).

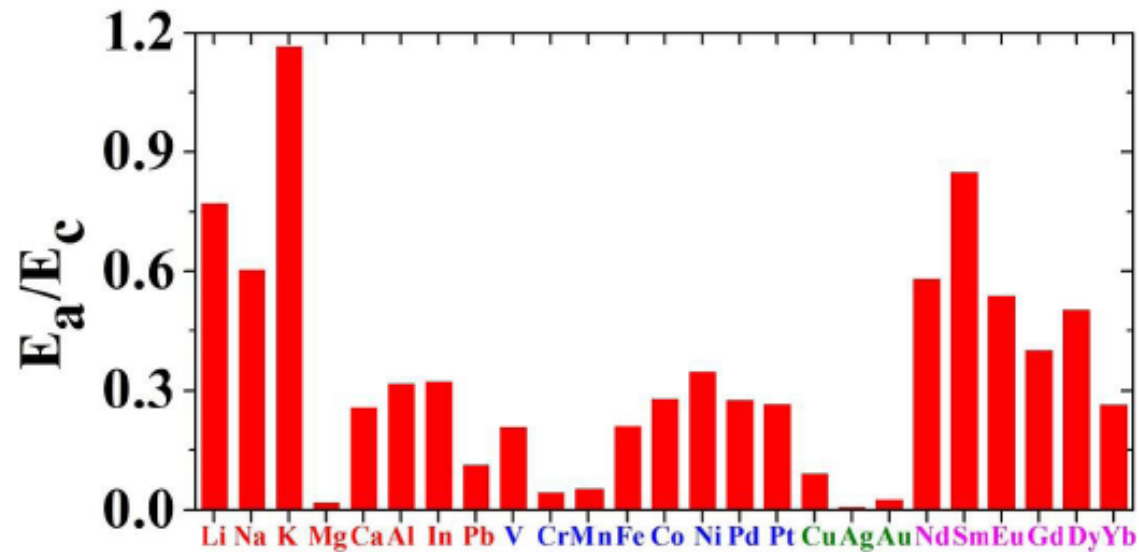


Figura 1.24: Il rapporto $\frac{E_a}{E_c}$ [19].

Nelle Fig.1.25 e Fig.1.26 sono mostrate le simulazioni della densità di carica elettronica (eq.4.15): il color Oro indica una forte densità di carica ($\Delta p > 0$), l'azzurro indica una bassa densità di carica ($\Delta p < 0$) e il viola indica inalterata la densità di carica ($\Delta p = 0$). Si osserva, in particolare, che l'Argento al di sopra del Grafene non modifica la densità elettronica di quest'ultimo ($\Delta p = 0$).

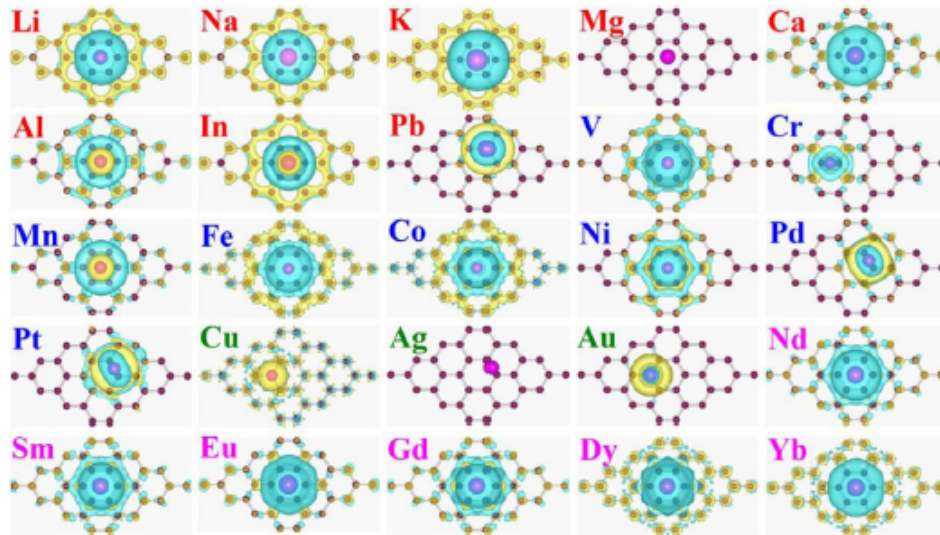
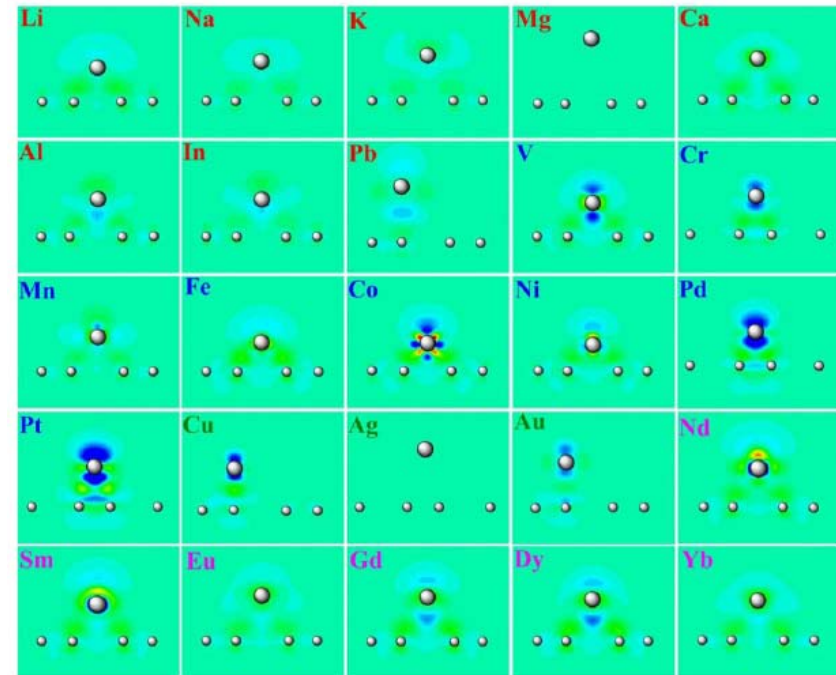


Figura 1.25: La densità elettronica di vari atomi al di sopra del Grafene vista dall'alto. Il color Oro indica una forte densità di carica ($\Delta p > 0$), l'azzurro indica una bassa densità di carica ($\Delta p < 0$) e il viola indica inalterata la densità di carica ($\Delta p = 0$) [20].

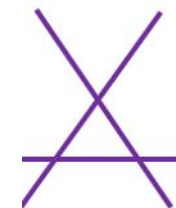


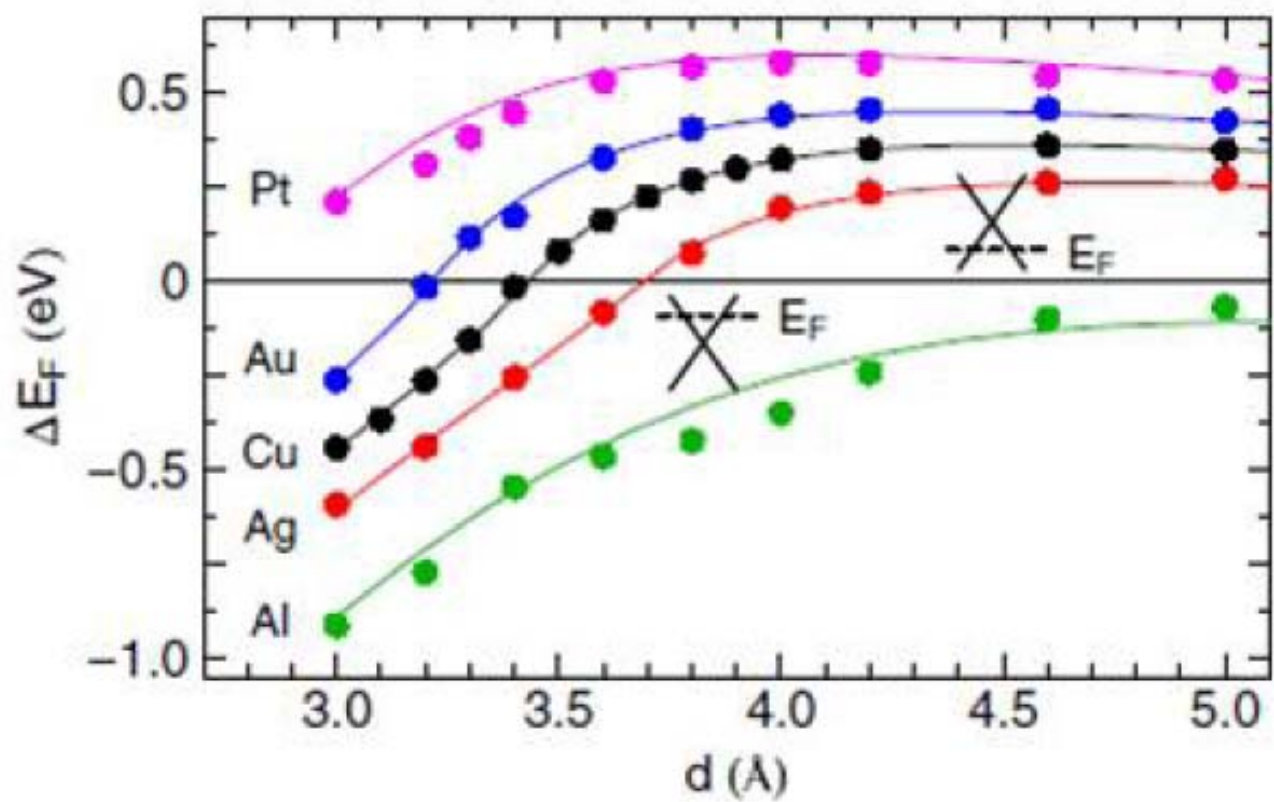
	Gr	Ni	Co	Pd	Al	Ag	Cu	Au	Pt
d_{eq} (Å)		2.05	2.05	2.30	3.41	3.33	3.26	3.31	3.30
ΔE (eV)		0.125	0.160	0.084	0.027	0.043	0.033	0.030	0.038
W_M (eV)		5.47	5.44	5.67	4.22	4.92	5.22	5.54	6.13
W (eV)	4.48	3.66	3.78	4.03	4.04	4.24	4.40	4.74	4.87

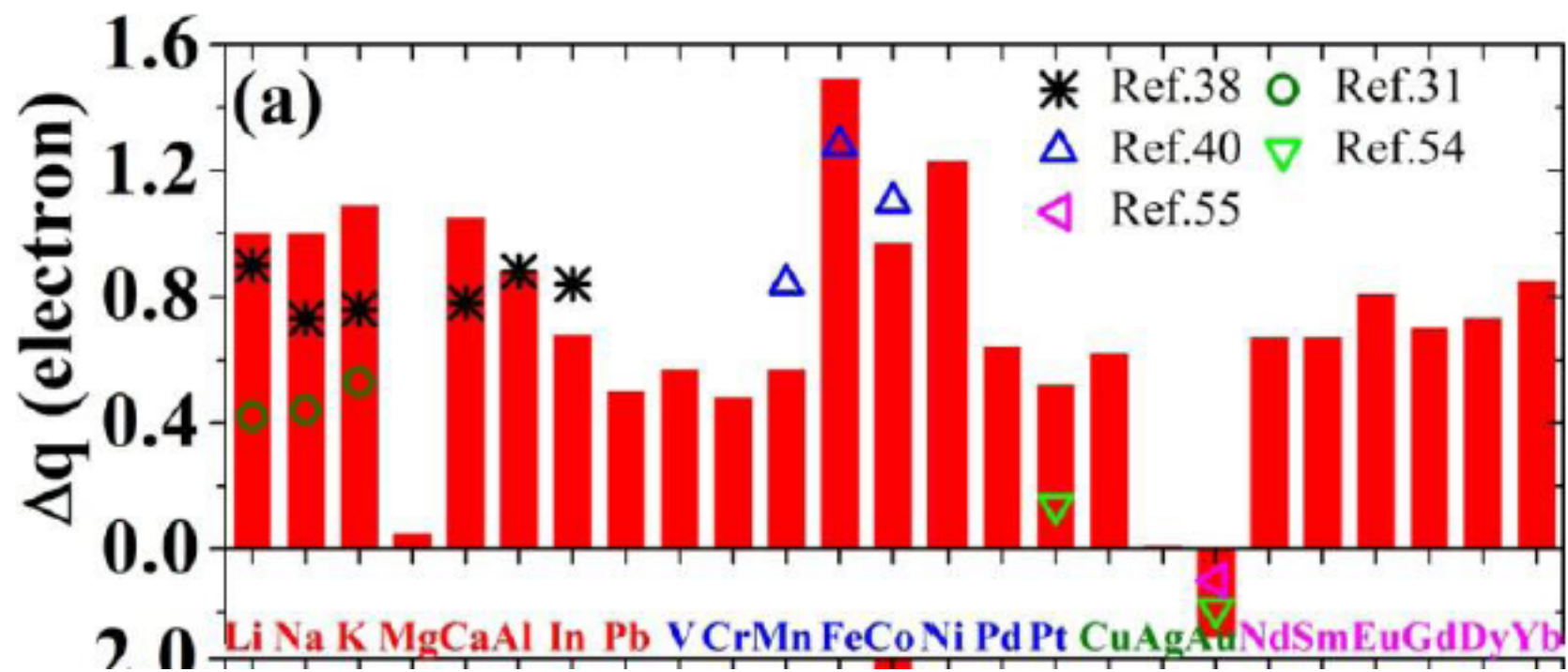
Tabella 1.1: Alcune caratteristiche del contatto Metallo-Grafene. d_{eq} é la distanza di equilibrio fra il metallo e il Grafene; ΔE é l'energia di legame; W_M é il potenziale di estrazione del metallo; W é il potenziale di estrazione del Grafene sia free-standing (verrà indicato con $W_G = 4.48$ eV) e sia nel caso in cui esso é drogato a causa dell'interazione con uno specifico metallo [22].

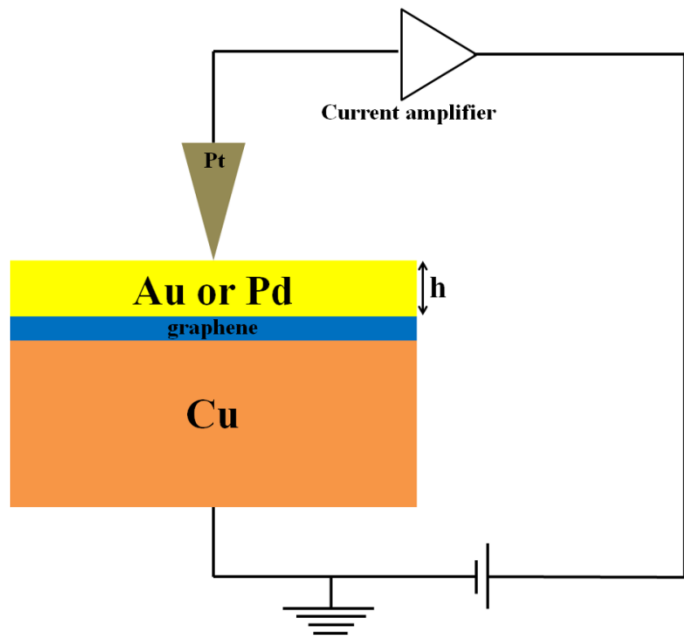
La presenza del metallo a contatto con il Grafene determina un drogaggio di quest'ultimo, perché esso varia il suo potenziale di estrazione. Il tipo di drogaggio a cui è sottoposto il Grafene dipende da vari fattori che porteranno ad una variazione del suo potenziale di estrazione (W):

- Se $W < W_G$ (potenziale di estrazione del Grafene free-standing) il Grafene si droga di tipo n , cioè la concentrazione di elettroni è maggiore rispetto a quello free-standing, questo perché il livello di Fermi si trova al di sopra del punto di Dirac (come si evince dalla Fig.1.29c) [22].
- Se $W \cong W_G$ il Grafene si comporta come un metallo [22].
- Se $W > W_G$ il Grafene si droga di tipo p , cioè la concentrazione di elettroni è minore rispetto a quello free-standing, questo perché il livello di Fermi si trova al di sotto del punto di Dirac (Fig.1.28) [22].

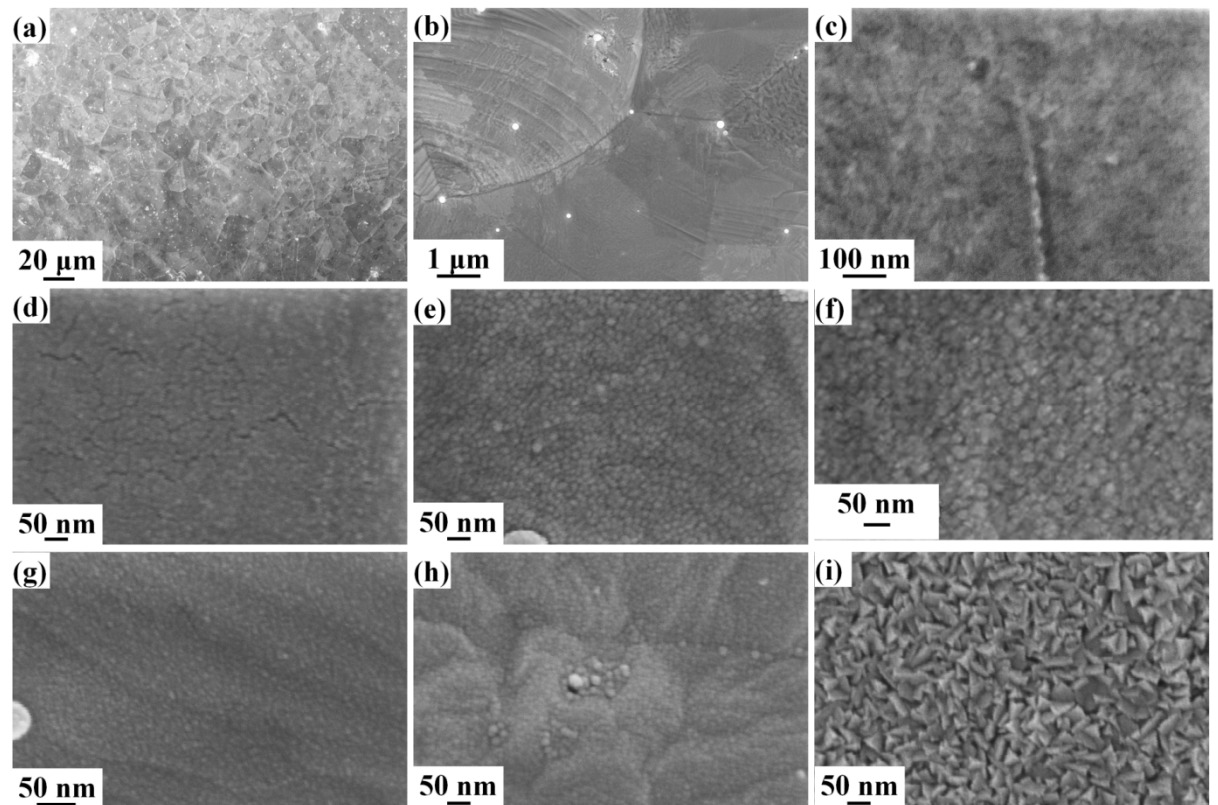


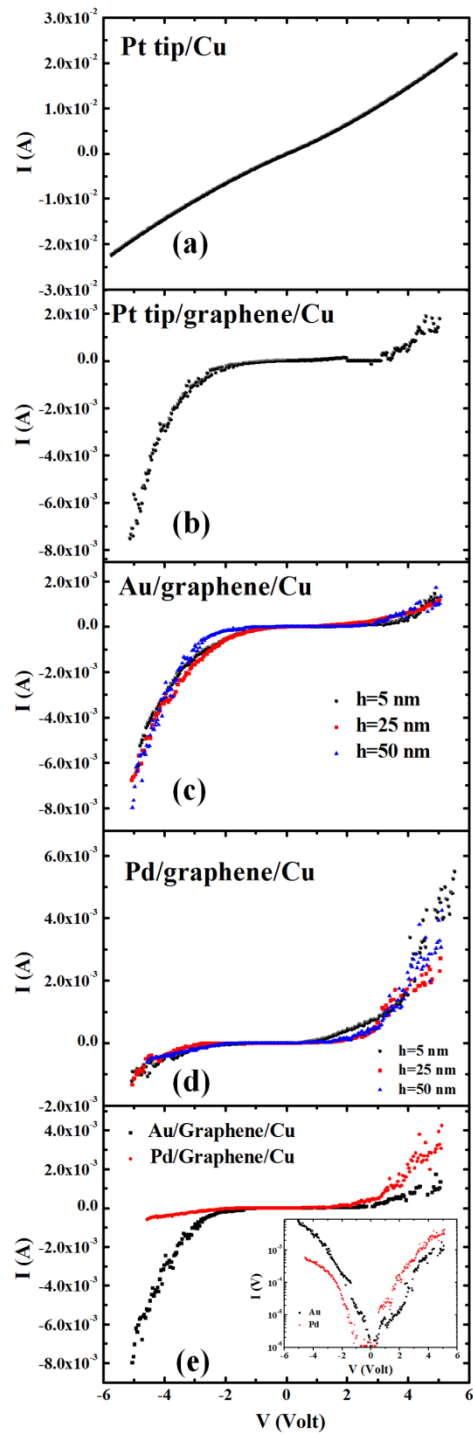




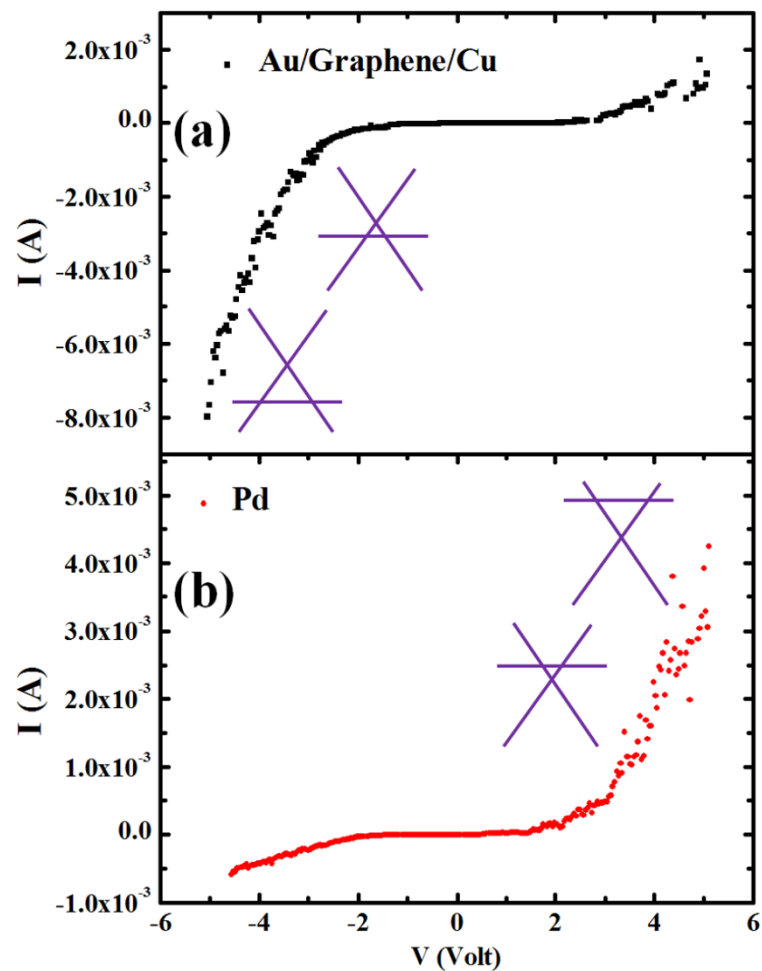


Representative scanning electron microscopy images of: (a)-(c) graphene/Cu surface at different magnifications; (d)-(f) Au films deposited on the graphene/Cu surface with thickness of 5 nm (d), 25 nm (e), and 50 nm (f); (g)-(i) Pd films deposited on the graphene/Cu surface with thickness of 5 nm (g), 25 nm (h), and 50 nm (i).





	Gr	Ni	Co	Pd	Al	Ag	Cu	Au	Pt
d_{eq} (Å)		2.05	2.05	2.30	3.41	3.33	3.26	3.31	3.30
ΔE (eV)		0.125	0.160	0.084	0.027	0.043	0.033	0.030	0.038
W_M (eV)		5.47	5.44	5.67	4.22	4.92	5.22	5.54	6.13
W (eV)	4.48	3.66	3.78	4.03	4.04	4.24	4.40	4.74	4.87



Question 3: Quantum Hall Effect

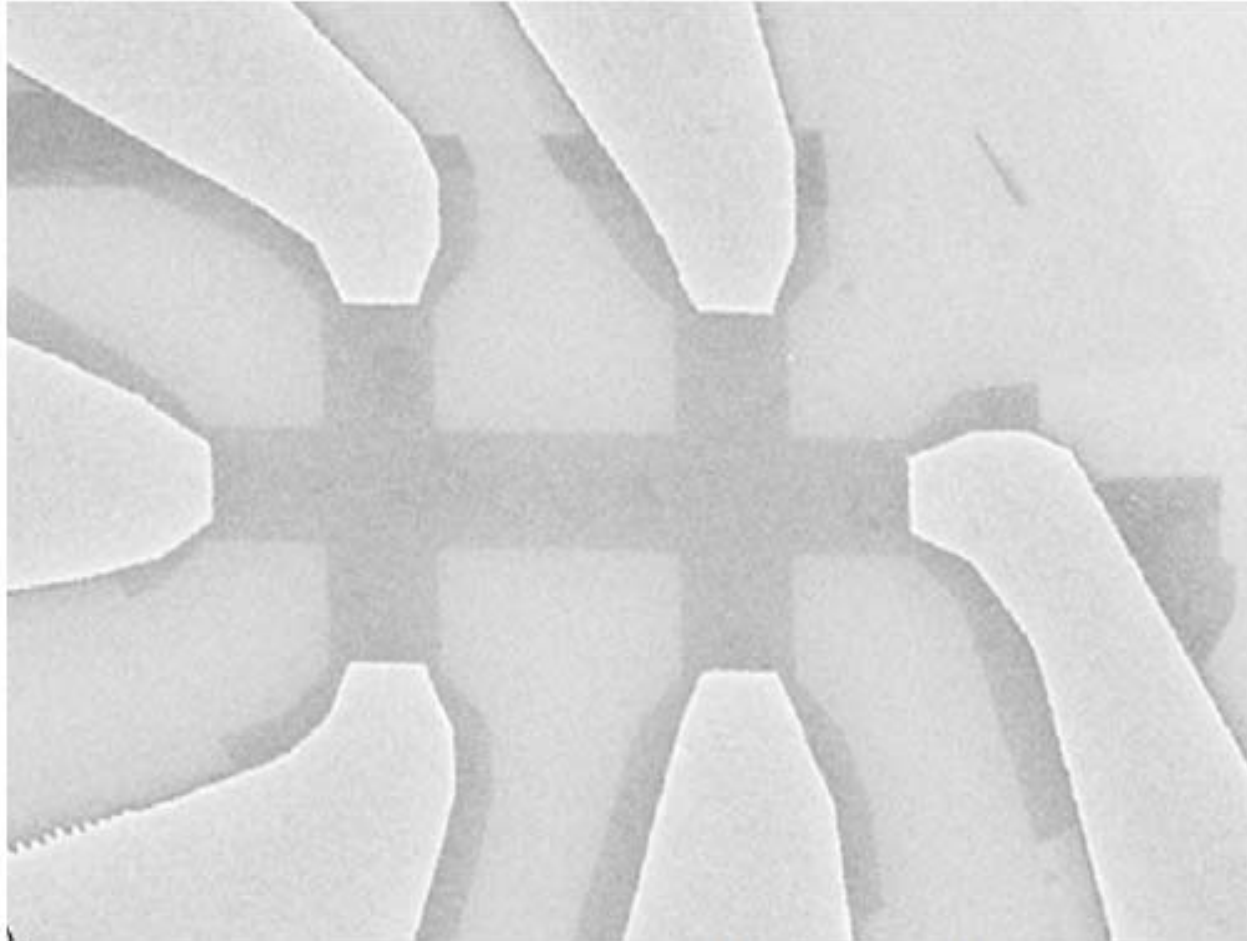
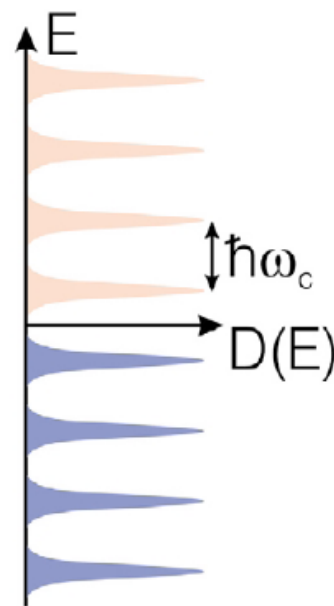


Fig. 5 Scanning electron micrograph of a graphene device. The graphene crystal is contacted by Au electrodes and patterned into Hall bar geometry by e-beam lithography with subsequent reactive plasma etching. The width of the channel is 1 μm . (Courtesy of K. Novoselov and A. Geim.)

Anomalous quantum Hall effect

Magneto-oscillation effects, such as the de Haas-van Alphen (oscillations of magnetization) or Schubnikov-de Haas (magneto-oscillations in resistance) effects, are among the most straightforward and reliable tools to investigate electron energy spectra in metals and semiconductors³⁵. In two-dimensional systems with a constant magnetic field \mathbf{B} perpendicular to the system plane, the energy spectrum is discrete (Landau quantization). In the case of massless

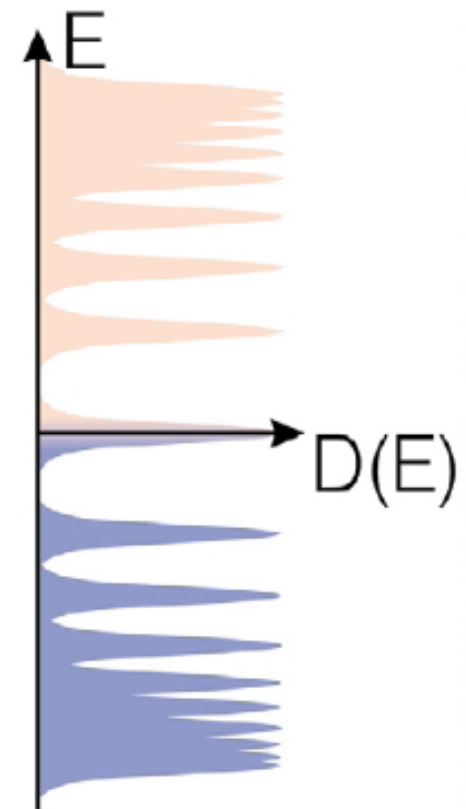


Dirac fermions, the energy spectrum takes the form (see³⁶, for example):

$$E_{\nu\sigma} = \pm \sqrt{2 |e| B \hbar v_F^2 (\nu + 1/2 \pm 1/2)} \quad (1)$$

where v_F is the electron velocity, $\nu = 0, 1, 2, \dots$ is the quantum number, and the term with $\pm 1/2$ is connected with the chirality (Fig. 6). For comparison, in the usual case of a parabolic dispersion relation, the Landau level sequence is $E = \hbar\omega_c (\nu + 1/2)$ where ω_c is the frequency of electron rotation in the magnetic field (cyclotron frequency)³⁵.

By changing the value of the magnetic field at a given electron concentration (or, vice versa, electron concentration for a given magnetic field), one can tune the Fermi energy E_F to coincide with one of the Landau levels. This drastically changes all properties of metals (or semiconductors) and, thus, different physical quantities will oscillate with the value of the inverse magnetic field. By measuring the period



An important peculiarity of the Landau levels for massless Dirac fermions is the existence of zero-energy states (with $\nu = 0$ and a minus sign in eq. 1). This situation differs markedly from conventional semiconductors with parabolic bands where the first Landau level is shifted by $\frac{1}{2}\hbar\omega_c$. As shown by the Manchester and Columbia groups^{15,16}, the existence of the zero-energy Landau level leads to an anomalous QHE with *half-integer* quantization of the Hall conductivity (Fig. 8, top), instead of an *integer* one (for a review of the QHE, see³⁷, for example). Usually, all Landau levels have the same degeneracy (number of electron states with a given energy), which is proportional to the magnetic flux through the system. As a result, the plateaus in the Hall conductivity corresponding to the filling of first ν levels are integers (in units of the conductance quantum e^2/h). For the case of massless Dirac electrons, the zero-energy Landau level has half the degeneracy of any other level (corresponding to the minus sign in eq. 1), whereas each p^{th} level with $p \geq 1$ is obtained twice, with $\nu = p$ and a minus sign, and with $\nu = p - 1$ and a plus sign. This anomalous QHE is the most direct evidence for Dirac fermions in graphene^{15,16}.

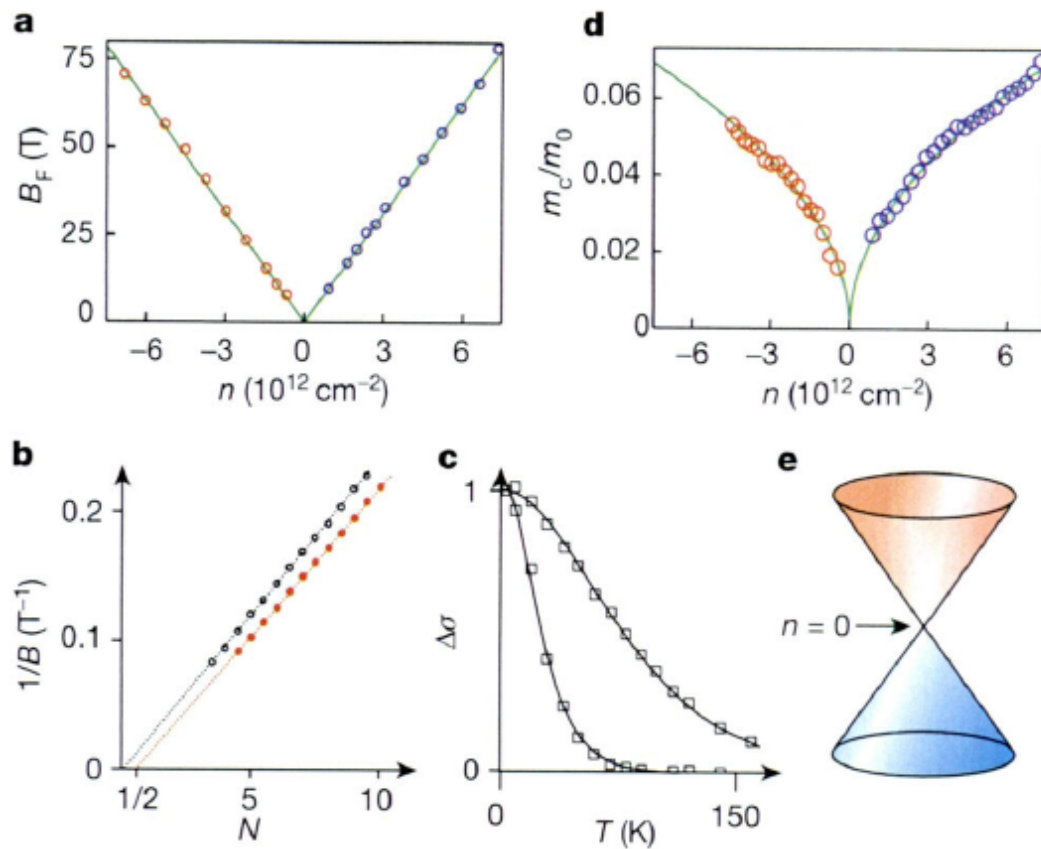


Figure 3 | Dirac fermions of graphene. **a**, Dependence of B_F on carrier concentration n (positive n corresponds to electrons; negative to holes). **b**, Examples of fan diagrams used in our analysis⁷ to find B_F . N is the number associated with different minima of oscillations. The lower and upper curves are for graphene (sample of Fig. 2a) and a 5-nm-thick film of graphite with a similar value of B_F respectively. Note that the curves extrapolate to different origins, namely to $N = 1/2$ and $N = 0$. In graphene, curves for all n extrapolate to $N = 1/2$ (compare ref. 7). This indicates a phase shift of π with respect to the conventional Landau quantization in metals. The shift is due to Berry's phase^{14,20}. **c**, Examples of the behaviour of SdHO amplitude $\Delta\sigma$ (symbols) as a function of T for $m_c \approx 0.069$ and $0.023m_0$ (see the dependences showing the rapid and slower decay with increasing T , respectively); solid curves are best fits. **d**, Cyclotron mass m_c of electrons and holes as a function of their concentration. Symbols are experimental data, solid curves the best fit to theory. **e**, Electronic spectrum of graphene, as inferred experimentally and in agreement with theory. This is the spectrum of a zero-gap 2D semiconductor that describes massless Dirac fermions with $c \cdot 1/300$ the speed of light.

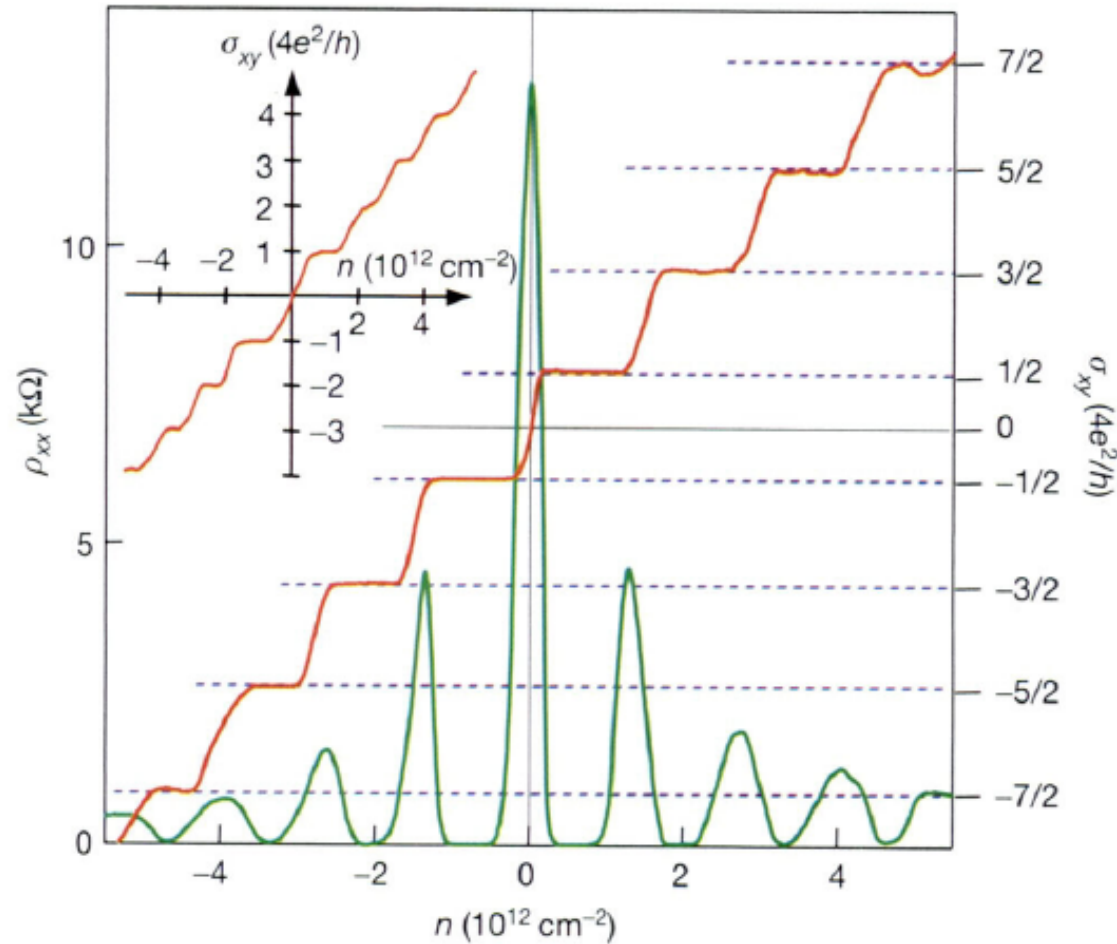
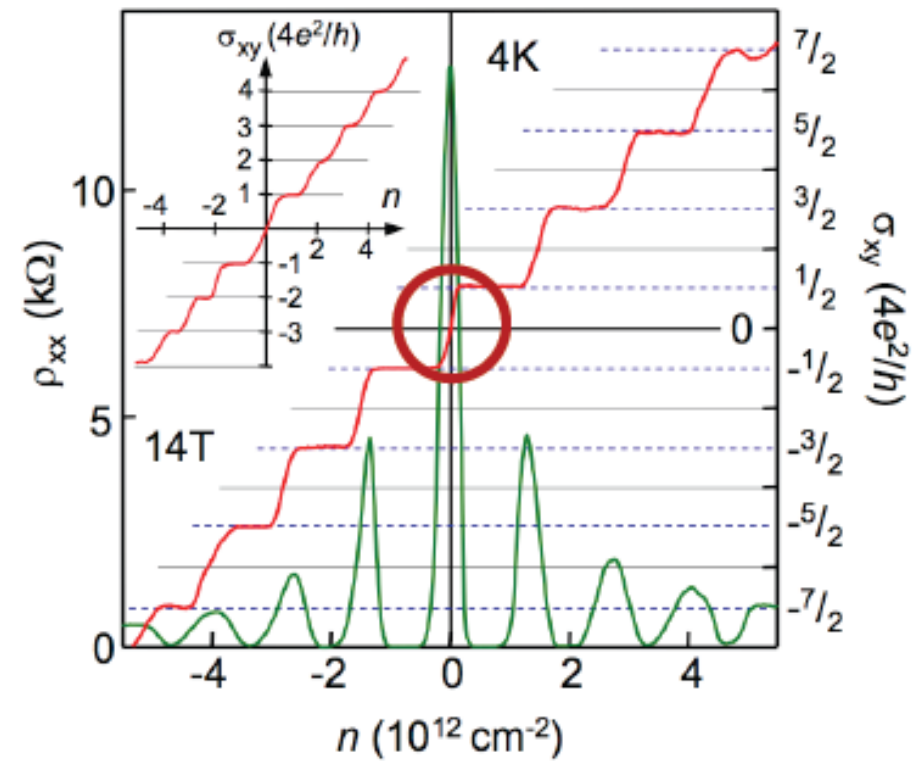
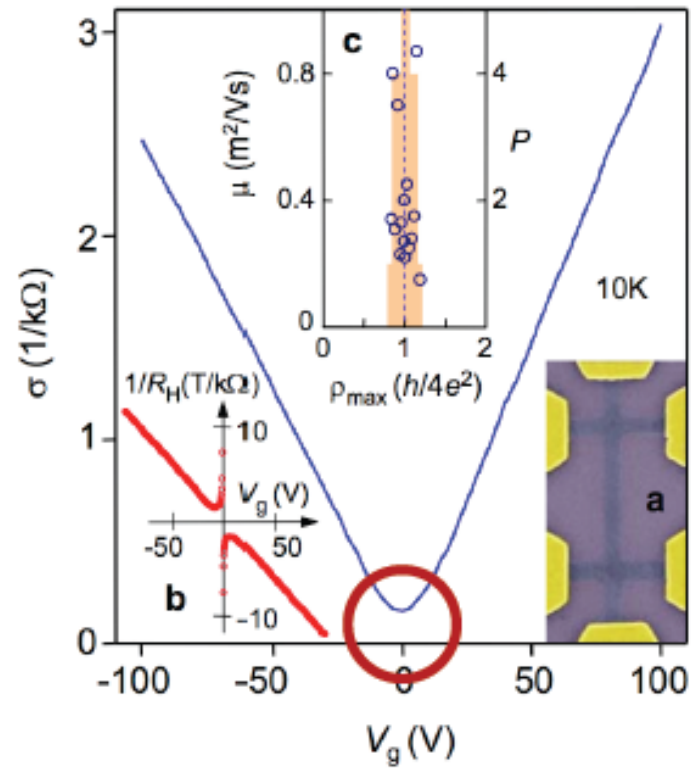


Figure 4 | QHE for massless Dirac fermions. Hall conductivity σ_{xy} and longitudinal resistivity ρ_{xx} of graphene as a function of their concentration at $B = 14$ T and $T = 4$ K. $\sigma_{xy} \equiv (4e^2/h)\nu$ is calculated from the measured dependences of $\rho_{xy}(V_g)$ and $\rho_{xx}(V_g)$ as $\sigma_{xy} = \rho_{xy}/(\rho_{xy}^2 + \rho_{xx}^2)$. The behaviour of $1/\rho_{xy}$ is similar but exhibits a discontinuity at $V_g \approx 0$, which is avoided by plotting σ_{xy} . Inset: σ_{xy} in 'two-layer graphene' where the quantization sequence is normal and occurs at integer ν . The latter shows that the half-integer QHE is exclusive to 'ideal' graphene.



- minimal conductance of $O(\text{conductance quantum})$
- quantum Hall effect with plateau quantization $\sigma_{xy} = (2e^2/h)(2n + 1)$

K. Von Klitzing

Io (più giovane,
2006)



Fine

Graphene has a honeycomb lattice shown in Figure 3.4 using a *ball-and-stick* model. The balls represent carbon atoms and the sticks symbolize the σ -bonds between atoms. The carbon–carbon bond length is approximately $a_{C-C} \approx 1.42 \text{ \AA}$. The honeycomb lattice can be characterized as a Bravais lattice with a basis of two atoms, indicated as A and B in Figure 3.4, and these contribute a total of two π electrons per unit cell to the electronic properties of graphene. The underlying Bravais lattice is a hexagonal lattice and the primitive unit cell can be considered an equilateral parallelogram with side $a = \sqrt{3}a_{C-C} = 2.46 \text{ \AA}$. The primitive unit vectors as defined in Figure 3.4 are

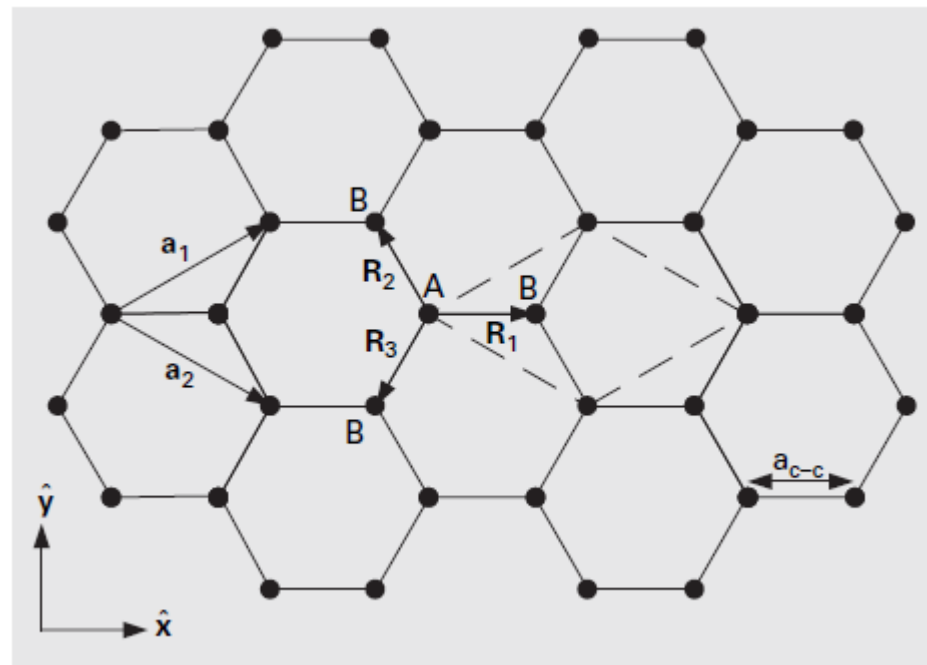
$$\mathbf{a}_1 = \left(\frac{\sqrt{3}a}{2}, \frac{a}{2} \right), \quad \mathbf{a}_2 = \left(\frac{\sqrt{3}a}{2}, \frac{a}{-2} \right), \quad (3.1)$$

with $|\mathbf{a}_1| = |\mathbf{a}_2| = a$. Each carbon atom is bonded to its three nearest neighbors

and the vectors describing the separation between a type A atom and the nearest neighbor type B atoms as shown in Figure 3.4 are

$$\begin{aligned} \mathbf{R}_1 &= \left(\frac{a}{\sqrt{3}}, 0 \right), \mathbf{R}_2 = -\mathbf{a}_2 + \mathbf{R}_1 = \left(-\frac{a}{2\sqrt{3}}, -\frac{a}{2} \right), \\ \mathbf{R}_3 &= -\mathbf{a}_1 + \mathbf{R}_1 = \left(-\frac{a}{2\sqrt{3}}, \frac{a}{2} \right), \end{aligned} \quad (3.2)$$

with $|\mathbf{R}_1| = |\mathbf{R}_2| = |\mathbf{R}_3| = a_{C-C}$.

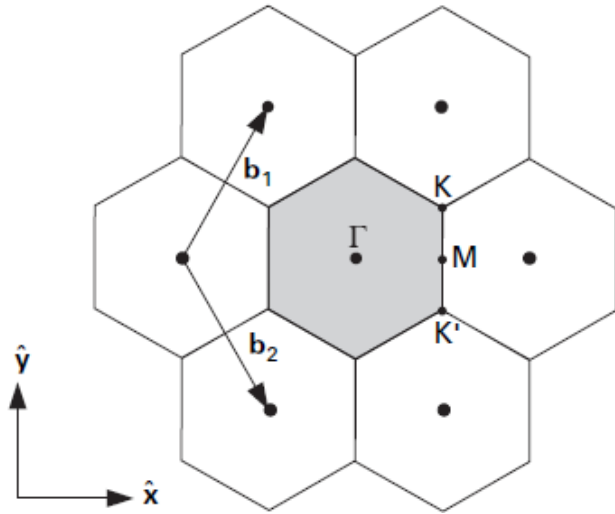


The reciprocal lattice of graphene shown in Figure 3.5 is also a hexagonal lattice, but rotated 90° with respect to the direct lattice. The reciprocal lattice vectors are (from Eq. (2.34))

$$\mathbf{b}_1 = \left(\frac{2\pi}{\sqrt{3}a}, \frac{2\pi}{a} \right), \quad \mathbf{b}_2 = \left(\frac{2\pi}{\sqrt{3}a}, -\frac{2\pi}{a} \right), \quad (3.3)$$

with $|\mathbf{b}_1| = |\mathbf{b}_2| = 4\pi/\sqrt{3}a$. The Brillouin zone, which is a central idea in describing the electronic bands of solids, is illustrated as the shaded hexagon in Figure 3.5 with sides of length $b_{BZ} = |\mathbf{b}_1|/\sqrt{3} = 4\pi/3a$ and area equal to $8\pi^2/\sqrt{3}a^2$. There are three key locations of high symmetry in the Brillouin zone which are useful to memorize in discussing the dispersion of graphene. In Figure 3.5, these locations are identified by convention as the Γ -point, the M-point, and the K-point.³ The Γ -point is at the center of the Brillouin zone, and the vectors describing the location of the other points with respect to the zone center are

$$\Gamma M = \left(\frac{2\pi}{\sqrt{3}a}, 0 \right), \quad \Gamma K = \left(\frac{2\pi}{\sqrt{3}a}, \frac{2\pi}{3a} \right), \quad (3.4)$$



Tight-binding energy dispersion

$$\Psi(\mathbf{k}, \mathbf{r}) = C_A \Phi_A(\mathbf{k}, \mathbf{r}) + C_B \Phi_B(\mathbf{k}, \mathbf{r}),$$

$$\Phi_A(\mathbf{k}, \mathbf{r}) = \frac{1}{\sqrt{N}} \sum_j^N e^{i\mathbf{k} \cdot \mathbf{R}_{A_j}} \phi(\mathbf{r} - \mathbf{R}_{A_j}) \quad (3.10)$$

$$\Phi_B(\mathbf{k}, \mathbf{r}) = \frac{1}{\sqrt{N}} \sum_j^N e^{i\mathbf{k} \cdot \mathbf{R}_{B_j}} \phi(\mathbf{r} - \mathbf{R}_{B_j}), \quad (3.11)$$

where N is the number of unit cells in the lattice and $\mathbf{R}_A(\mathbf{R}_B)$ are the Bravais lattice vectors identifying the locations of all type A (B) atoms in the graphene lattice. The atomic orbitals ϕ belong to a class of functions known as Wannier functions, which are orthonormal functions that are sufficiently localized such that, at distances increasingly removed from the center point \mathbf{R}_j , the functions decay to zero very rapidly. The sum is over all the lattice vectors, and $1/\sqrt{N}$ serves as normalization constant for the Bloch functions in the strict limit when the Wannier function in cell j has zero overlap with neighboring Wannier functions.⁸